Journal of Materials Chemistry A

Accepted Manuscript

ROYAL SOCIETY OF CHEMISTRY

www.rsc.org/materialsA

Journal Name

ARTICLE

Precisely Tailoring ZIF-67 Nanostructures from Cobalt Carbonate Hydroxide Nanowire Arrays: Toward High-Performance Battery-Type Electrodes

Received 00th January 20xx,
Accepted 00th January 20xx

DOI: 10.1039/x0xx00000x

www.rsc.org/

Dongbo Yu,[a] Liang Ge,[a] Bin Wu,[a] Liang Wu,[a] Huanting Wang [b] and Tongwen Xu[*, a]

The controllable synthesis of metal organic frameworks with diverse morphologies is highly desirable for many potential applications, but it still remains a big challenge. In this study, we for the first time report a facile and green route for the synthesis of ZIF-67 at room temperature by transformation of water-insoluble cobalt carbonate hydroxide nanowires in the presence of 2-methylimidazole. When cobalt carbonate hydroxide nanowires were grown onto a Ni foam substrate, four different kinds of ZIF67 nanocrystal morphologies were synthesized. In particular, ZIF-67-based nanotube array was used as an example for synthesis of mesoporous Co_3O_4 nanotube array, which showed greatly enhanced performance as battery-type electrode in comparison to the directly converted Co_3O_4 nanowire array from cobalt carbonate hydroxide. Our study provides a new insight into the preparation of metal organic framework with tunable morphologies; in addition, the as-synthesized ZIF-67-based nanostructures are promising materials for other applications.

Introduction

Metal-organic frameworks (MOFs) constructed by coordination bonds between organic linkers and metal ions represent an important class of porous crystalline materials.[1-3] Owing to the high porosity and surface area as well as the unique structural and functional flexibility, the surge of tide in MOF research is sweeping over a wide range of application fields including gas separation and storage,[4-8] catalysts,[9-11] sensors[12] and energy technologies.[13-20] It has been reported that MOFs-derived metal oxide/graphene network composites show promising performances in photocatalysis and lithium-ion battery due to their mesoporous morphologies of metal oxides and three dimensional heterostructure of composites.[16]

The size, morphology and architecture of materials affect their physicochemical and electrochemical properties significantly.[8, 21-25] In general, it is preferable to use high-aspect-ratio structured nanowires/nanotubes or nanosheets rather than nanoparticles as active materials in battery electrodes because of desirable dispersibility, accessible charge transfer and superior stability.[22, 24] After decades of extensive research, a variety of nanostructures have been exploited through different specific approaches. However, despite great potential of MOFs, particle-like shape has been the dominant morphology, and the lack of variety and multiplicity in morphology hinders the broader applications of MOFs and their derivatives. Recently, MOFs in the form of freestanding nanosheets incorporated into polymer matrix enable outstanding CO_2 separation performance, which is attributed to the more favorable assembly of MOF nanosheet fillers in the membrane cross-section, resulting in the enhanced efficiency of gas discrimination and elimination of non-selective permeation pathway.[8] It demonstrates that there is an urgent need to explore new strategy for addressing the challenges in controlling morphologies of MOFs.

It is found that the simple capillary could induce the directional self-assembly of MOF particles through facet-to-facet attractions between them.[26] On the basis of this research, locked MOF particle chains are further achieved with the assistance of an external electric field. Nevertheless, it is unsatisfying because the building blocks have to be polyhedral MOF crystals with flat facets those normally have very big particle size (~ μm-scale).[27] Different from conventional method of MOF synthesis, some reported studies have manifested the possibility to use inorganic crystals as metal ion sources. A mechanochemical conversion method has been proved to be a reliable way of synthesizing ZIF-8 by using ZnO as the Zn source, and it gives rise to a ZnO@ZIF-8 core-shell structure.[28] In the synthesis of HKUST-1 ($Cu_3(btc)_2$, btc=1,3,5-benzenetricarboxylate), $Cu(OH)_2$ serves as precursor material, the acid-base interaction of $H_3btc/Cu(OH)_2$ ensures the fast crystallization kinetics, and the full conversion to HKUST-1 is completed after 1 h in a water-ethanol media.[29] Together with the consideration of sacrificial-template approach, in which as-prepared nano-structures act as both of the precursors and

[a] CAS Key Laboratory of Soft Matter Chemistry, Collaborative Innovation Center of Chemistry for Energy Materials, School of Chemistry and Material Science, University of Science and Technology of China, Hefei 230026, P.R. China. Email Address: twxu@ustc.edu.cn
[b] Department of Chemical Engineering, Monash University, Clayton, Victoria 3800, Australia.
† Electronic Supplementary Information (ESI) available: See
DOI: 10.1039/x0xx00000x

templates and the original template shapes could be tuned with controllable hierarchically structures,[30-33] applying the similar approach to MOF synthesis is thus reasonable when a proper template is chosen and the conversion is well manipulated.

In this study, we for the first time demonstrate that nanostructured ZIF-67 with different morphologies can be precisely synthesized from crystalline cobalt carbonate hydroxide nanowires (Co-NWs) in aqueous solution, without involving toxic organic solvents. By carefully controlling experimental conditions (temperature, reaction time and concentration of solution), cobalt carbonate hydroxide nanowire array (Co-NWA) aligned on Ni foam is subsequently converted into different ZIF-67-based nanostructures including bead-on-string morphology, core-shell structure, nanoflake and nanotube. To demonstrate the potential applications of these nanostructures, as an example, the resulting ZIF-67 nanotube array (ZIF-NTA) is used to generate mesoporous Co_3O_4 nanotube array (Co_3O_4-NTA) under heat treatment. Very interestingly, the ZIF-67-derived Co_3O_4-NTA exhibits much higher specific capacity, better rate capability and stability than the Co_3O_4 nanowire array (Co_3O_4-NWA) directly converted from Co-NWs. Our work provides a new and effective way to precisely tailor MOF-based nanostructures, and significantly extends the functionality and applications of MOFs.

Results and discussion

In our work, Co-NWs were prepared by a typical hydrothermal method (Supporting Information). The conversion of Co-NWs into ZIF-67 was carried out in 2-methylimidazole (HMe-Im) aqueous solution at room temperature. Figure 1a shows the scanning electron microscopy (SEM) image of the Co-NW, the nanowires have a single-crystal structure (Figure S1). After 24 h synthesis, polyhedral ZIF-67 particles (~ 1 μm in size) emerged (Figure 1b) and they were strung on Co-NWs forming a bead-on-string structure (indicated by red arrows, Figure 1b). Prolonging the synthesis time to 7 days, the particles grew up into large crystals with the sizes of 2 ~ 5 μm. The crystal growth was possibly due to Ostwald ripening although some nanowire residues were observed (indicated by blue circles, Figure 1c). These results indicate that the reaction between cobalt carbonate hydroxide and HMe-Im is quite slow in comparison with that of severe acid-base reaction in previous HKUST-1 synthesis.[29] When triethylamine (TEA) was added, pure ZIF-67 with smaller particle sizes was produced; its size distribution ranged from several tens to hundreds of nanometers (Figure 1d). This's because TEA deprotonated HMe-Im to induce more ZIF-67 nuclei and accelerate its crystallization process.[34] The X-ray diffraction (XRD) results in Figure S2 were in agreement with the SEM observation, the peaks of cobalt carbonate hydroxide could not be detected after 7-day reaction with addition of TEA indicating the complete conversion of ZIF-67. In addition, there was almost no cobalt carbonate hydroxide nanowire residue observed in the transmission electron microscopy (TEM) image (Figure S3a), small-size and big-size ZIF-67 coexisted together in the resulting product. Thermal gravity analysis (TGA, Figure S3b) indicated the decomposition of HMe-Im of ZIF-67 crystals finished and retained ~ 67.8 % of initial weight; the weight loss in previous stage could be ascribed to the removal of water and some free Hme-Im attached in the nanopores of ZIF-67, the oxidation of residue carbon caused extreme loss from 350 to 420 ^{o}C in air, after that it remained 22.7 % of mass, suggesting the total conversion into Co_3O_4. The ZIF-67 samples synthesized at room temperature have Brunauer-Emmett-Teller (BET) surface area of 417.5 m^2/g (7 days in water) and 937.5 m^2/g (7 days in present of TEA) (Figure S4), which are comparable to previously reported values,[34-36] and the much lower BET surface area for the sample in absence of TEA should mainly result from the incomplete conversion of cobalt carbonate hydroxide nanowires inside the resulting powder.

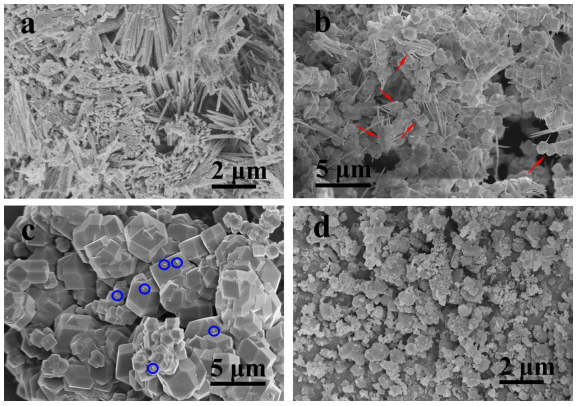

Figure 1. SEM images of the precursor Co-NWs (a) and resulting materials in aqueous solution at room temperature after different reaction time of 24 h (b), 7 days (c) and 7 days in addition of TEA (d).

In the conventional synthesis of ZIF-67, soluble Co salts such as nitrates, chlorides and acetates are used. In our case, it is interesting to see that the solvent-insoluble crystal cobalt carbonate hydroxide could serve as a Co source. The layered crystal structure of cobalt carbonate hydroxide in which CO_3^- ions are embedded between cobalt hydroxide nanosheets, allows the diffusion of H^+ ions, Hme-Im molecules and water inside cobalt carbonate hydroxide, inducing the breakage of Co-OH bond. Basic cobalt carbonate hydroxide would deprotonate HMe-Im, initiating the crystallization of ZIF67,[34, 37-38] as observed the strong acid-base interaction between $Cu(OH)_2$ and H_3btc that enables the growth of HKUST-1.[29] Due to its open framework, water molecules can freely transport into and out of ZIF-67, facilitating the diffusion and exchange of HMe-Im and Co-species (released by cobalt carbonate hydroxide). In addition, HMe-Im is continuously deprotonated by basic cobalt carbonate hydroxide, which dissociates and releases CO_3^{2-}, HCO_3^- and OH^- ions in water; the transformation of cobalt carbonate hydroxide into ZIF-67 hence continues until the precursor materials are consumed completely, the reaction involved in the system could be described as follows:

$$Co(CO_3)_{0.5}(OH)\cdot 0.11H_2O \rightarrow Co^{2+} + 0.5CO_3^{2-} + OH^- + 0.11H_2O$$

$$Co^{2+} + (2-x+y)HMe\text{-}Im \rightarrow [Co(min)_x(Me\text{-}Im)_y]^{x+} + (2-x)H^+$$

$$CO_3^{2-} + H^+ \rightarrow HCO_3^-$$

$$HCO_3^- + H^+ \rightarrow H_2CO_3 \rightarrow H_2O + CO_2 \uparrow$$

$$HCO_3^- + H_2O \rightarrow H_2CO_3 + OH^-$$

Surprisingly, when ethanol, methanol, dimethylform-amide or N-methyl-2-pyrrolidone replace water as the solvent, the pink Co-NWs powder doesn't turn into the violet colored ZIF-67 even though the temperature is increased up to 75°C (Figure S5). This should be because cobalt carbonate hydroxide does not dissociate in these solvents, and thus HMe-Im can not be deprotonated, indicating water plays a key role in the transformation process. It is noted that the transformation process occurs slowly, which offers an excellent opportunity to precisely control the crystallization process and thus tune ZIF67 morphologies.

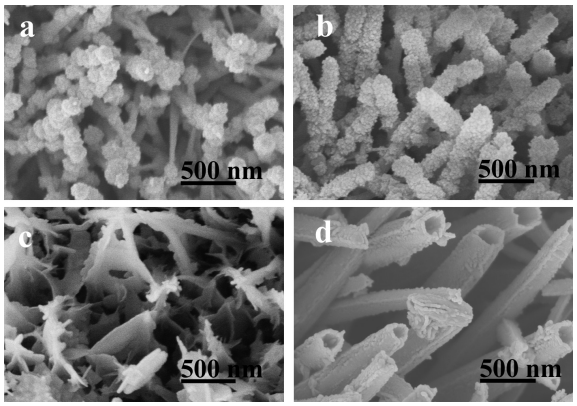

Figure 2. SEM images of ZIF-67-based materials originated from Co-NWA: bead-on-string nanowires (a), core-shell nanowires (b), nanoflakes (c) and nanotubes (d).

As observed in Figure 1b, some ZIF67 particles are grown on cobalt carbonate hydroxide nanowire to give the bead-on-string structure. However, too many Co^{2+} ions are released into the precursor solution; in the meantime, the organic linker HMe-Im among the interspaces of nanowire agglomerates is not able to consume all of Co^{2+} ions, thus free ZIF67 particles would crystallize in the precursor solution after long-range diffusion of these remnant Co^{2+} ions. To overcome this issue and realize more feasible control in the morphology of ZIF67-based structure, aligned Co-NWAs are applied, which enables desirable distribution of the building blocks for ZIF67 crystallization. More importantly, the well-ordered architectures are expected to facilitate favorable efficiency to electron transport and ion diffusion, leading to the enhanced performance in energy conversion and storage devices.[22, 39-44] Therefore, Two kinds of Co-NWAs, dense and relatively less-dense nanowire arrays were synthesized to build up three-dimensional ZIF-67-based nanostructures on a Ni foam (Figure S6), and finally four morphologies were obtained: in-situ growth of ZIF-67 nano-particles on Co-NW to form a bead-on-string structure (ZIF-67-NPs@Co-NW, Figure 2a), Co-NWs encapsulated by a layer of ZIF-67 (ZIF-67@Co-NW core-shell nanowire array, ZIF-CSNWA, Figure 2b), nanoflake cluster array (Figure 2c) and nanotube array (Figure 2d).

The synthesis parameters such as temperature, reaction time and concentration of precursor solution were investigated, and the results were shown in Figure S6-S10. It was clear to see the nucleation of ZIF-67 on Co-NWs (Figure S7a), growing up to big ZIF-67 nanoparticles and the generation of ZIF-67-NPs@Co-NW bead-on-string structure (Figure S7b-d). With increasing the temperature from room temperature to 50°C and 75°C (Figure S7-S9), the crystallization rate of ZIF-67 increased and the bead-on-string morphology tended to be a core-shell structure, stemming from the fast kinetics of transformation at high temperature that results in more ZIF-67 nuclei. If a low concentration of HMe-Im aqueous solution was used, the ZIF-67 crystallization would slow down (Figure S9-S10), a new type of spike bat-shaped nanowires emerged as the conversion lasted for a long time (Figure S10e-f). Because TEA accelerated the ZIF-67 conversion process, the core-shell nanowire could be further changed into hollow nanotubular structure due to the Kirkendall effect (Figure S11).[45] The detailed formation mechanism would be discussed below. Specifically, using dense Co-NWA as the precursor led to the formation of nanoflakes and the nanoflake array was orderly aligned on the Ni foam (Figure S12). Since some flocculent species were observed to wrap around the Co-NWs (Figure S13), which released Co^{2+} to link with HMe-Im and afforded sufficient nutrients for ZIF-67, the dipole-dipole interaction could easily overcome the molecular resistance in a narrow space between each Co-NW. It preferred planar growth induced by the surface tension gradient, as a result, the morphology of nanoflake was formed. The flocculent species were actually the metastable phase produced at the initial stage, these flocs had a low degree of crystallinity and no peak was detected in XRD. They were subsequently incubated into ZIF-67 crystals (Figure S14), which revealed the crystallization of ZIF-67 showed functional dependence on the nucleation time in accordance with the previous result.[46]

Co_3O_4 has been widely applied for active materials of battery-type electrodes due to its low cost, environmental friendliness and high theoretical capacitance.[21-22, 41, 44, 47-49] Moreover, ZIF-67 is a typical Co-containing MOF material that could achieve mesoporous cobalt oxide with ultrahigh surface area after specific annealing treatment.[12] Among various prepared ZIF-67-based structures, ZIF-NTA is chosen as an example to synthesize mesoporous Co_3O_4-NTA for battery-type electrodes. For comparison, ZIF-CSNWA- or Co-NWA-derived Co_3O_4 nanowire arrays are also prepared following the same procedures. Figure 3a and b show the SEM images of ZIF-CSNWA and ZIF-NTA, respectively. There are some of ZIF-67@Co-NW core-shell nanowires penetrating through the big ZIF-67 particles (Figure 3a), and more ZIF-67 particles are generated in the synthesis of ZIF-NTA (Figure 3b). After annealing at 350°C for 2 h in air, ZIF-67 nanoparticles are shrunk, only those tightly integrated with the nanowire array have been retained (Figure 3c, d). In addition, all of the nanowires, nanotubes and particles show the rough surface

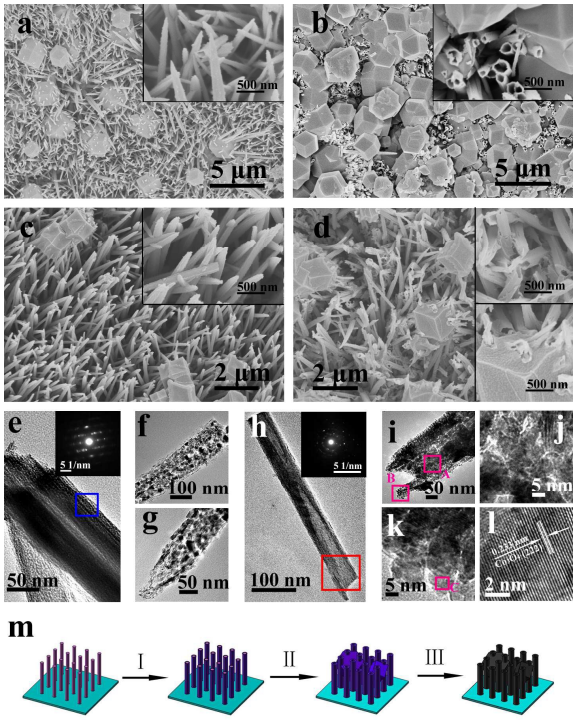

Figure 3. SEM images of ZIF-CSNWA (a), ZIF-NTA (b), Co_3O_4-CSNWA (c) and Co_3O_4-NTA (d); TEM images of ZIF-CSNWA (e), Co_3O_4-CSNWA (f, g), ZIF-NTA (h) and Co_3O_4-NTA (i); large-magnification TEM images of the rectangle area A (j) and area B (k); high-resolution TEM images of area C (l); schematic representation of the preparation of Co_3O_4-NWA on Ni foam (m). The insets in a-d show their corresponding enlarged images, the insets in e and h show the SAED patterns of the rectangle areas.

and the mesopores could be gleamingly observed. The XRD patterns of the samples before and after annealing (Figure S15) indicate their complete conversion to Co_3O_4 (JCPDS 42-1467) although both of ZIF-CSNWA and ZIF-NTA compose of two phase of ZIF-67 and cobalt carbonate hydroxide. Figure 3e, Figure S16 a and b show TEM images of ZIF-CSNWA, it is obvious to see that in the core-shell structure, the ZIF-67 shell is decorating on the surface of Co-NW core, and the corresponding selected area electron diffraction (SAED) spots (inset, Figure 3e) become dimmed compared with those of Co-NWs (Figure S1b) due to the formation of ZIF-67 with a poor crystallinity. ZIF-CSNWA-derived Co_3O_4-CSNWA remains the core-shell morphology (Figure 3f and g, Figure S16c and d). We can clearly see the much smaller particle size of shell (10 ~ 20 nm) than that for the Co-NW-derived Co_3O_4 core (40 ~ 50 nm), and the tip of ZIF-CSNWA is totally transformed into ZIF-67 so that the resulting Co_3O_4-CSNWA tip consists of very small nanoparticles (Figure 3g). TEM images shown in Figure 3h, Figure S16e and f display the tubular structure of as-synthesized Co_3O_4-NTA. The diffraction rings in the SAED pattern (inset, Figure 3h) reveal the polycrystalline structure of ZIF-67 nanotube. Residual cobalt carbonate hydroxide still exists inside the obtained nanotubes in terms of the appearance of regular diffraction spots (Figure S16h-j). The electron diffraction rings of ZIF-67 particle are lack of clarity, implying the relatively low crystallization degree at room temperature (Figure S16g). In addition, the annealing treatment of ZIF-67 particle results in the mesoporous Co_3O_4 nanoparticle (Figure S16k). The converted Co_3O_4 nanotube is composed of small nanoparticles with 10 ~ 20 nm in diameter (Figure 3i, Figure S16l and m), and narrow mesoporous channels inside the nanotube can be clearly observed (Figure 3j and h, area A and B in Figure 3i). The high-resolution TEM image of area C in Figure 3k shows the interplanar spacing of 0.233 nm, corresponding to the (222) plane of Co_3O_4 (Figure 3l). Co_3O_4-NTA has the highest BET surface area value of 31.8 m^2/g compared with 22.2 m^2/g for Co_3O_4-NWA and 23.3 m^2/g for Co_3O_4-CSNWA (Figure S16).

Based on the results and discussions above, the preparation of Co_3O_4-NTA is schematically illustrated in Figure 3m. Following with the in-situ growth on the Ni foam, Co-NWA was immersed into HMe-Im aqueous solution. Co-NWs on one hand afforded a basic environment to deprotonate HMe-Im due to the acid-base affinity; on the other hand, they provided Co-containing species such as Co^{2+} ions to link with the deprotonated HMe-Im, resulting in the initial metastable species. These species would transform into ZIF-67 crystals as it was a time-dependent process. The crystallization of ZIF-67 continuously proceeded with the consumption of metastable species, the surface of the Co-NWA was decorated by a layer of ZIF-67 and a core-shell structure was subsequently formed (process I, Figure 3m). Resulting from the fast kinetics of the transformation with addition of TEA to the precursor solution, the core-shell structure was further evolved into a tubular morphology as driven by the Kirkendall effect.[45] It was important to note that although cobalt carbonate hydroxide phase still remained in the prepared nanotubes in our case, actually the use of nanotubes or thinner nanowires was likely to achieve a pure phase since it facilitated the more desirable diffusion of building blocks. Because the released Co-containing species somewhere reached a high concentration but the crystallization rate of ZIF-67 was too slow to consume all of them, it preferred to generate the big crystalline ZIF-67 particles among the interspaces of Co-NWs (process II, Figure 3m). After the annealing treatment, ZIF-NTA was finally converted into Co_3O_4-NTA with very small Co_3O_4 nanoparticles and narrow mesoporous channels inside the nanotubes (process III, Figure 3m). Due to its specific structure which gives very small particle size with high surface area (Figure S17), Co_3O_4-NTA is expected to bring about remarkable capacitive performance in the use of battery-type electrodes.[50-52]

The electrochemical property of Co_3O_4-CSNWA and Co_3O_4-NTA were investigated in 2 M KOH aqueous solution as shown in Figure 4 and Figure S18. The cyclic voltammetry (CV) plots of Co_3O_4-NWA, Co_3O_4-CSNWA and Co_3O_4-NTA typically displayed a pair of peaks A/A' corresponding to the Co^{2+}/Co^{3+} redox couple (Figure 4a, Figure S18a-c).[22] The enclosed area of CV plot for Co_3O_4-NTA was the largest at a scan rate of 2 mV/s, revealing the highest capacity due to its unique structure (Figure 4a). In addition, Co_3O_4-NTA exhibited 2.92, 2.29, 1.79, 1.4 and 1.28 C/cm^2 of area capacity by varying the scan rate from 2 to 5, 10, 20 and 50 mV/s, respectively (Figure S18d). The galvanostatic charge-discharge measurements were also

carried out to further estimate the electrochemistry performance of as-prepared electrodes. Figure 4b, Figure S18 e and f were the corresponding galvanostatic charge–discharge curves of the electrodes as a function of the current density. Since Co_3O_4-NTA had the biggest surface area (Figure S17) and smallest particle size (Figure 3), which thus offered more active sites and shorter diffusion path for the Faradic effect reaction to store charges. At a current density of 2 mA/cm^2, it showed the highest area capacity of 2.26 C/cm^2 compared to 1.85 C/cm^2 of Co_3O_4-NWA and 2.09 C/cm^2 of Co_3O_4-CSNWA (Figure 4c), agreeing with the above CV results.

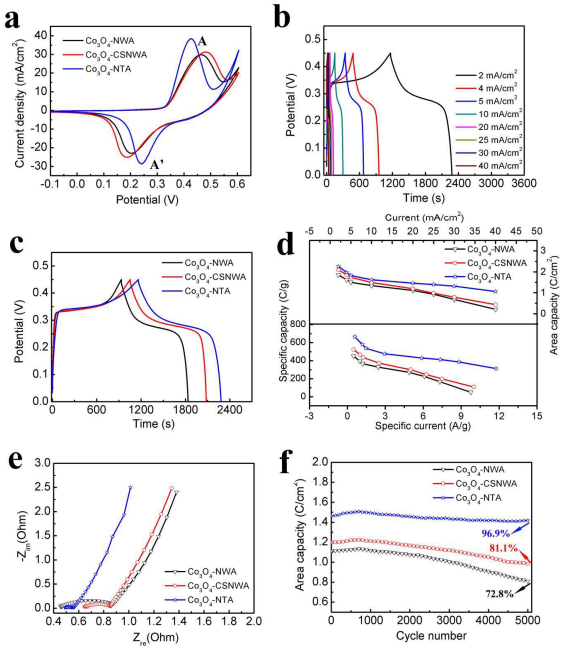

Figure 4 CV plots of Co_3O_4-NWA, Co_3O_4-CSNWA and Co_3O_4-NTA at the scan rate of 2 mV/s (a); galvanostatic charge-discharge curves of Co_3O_4-NTA at the current density of 2, 4, 5, 10, 20, 25, 30 and 40 mA/cm^2 (b); galvanostatic charge-discharge curves of Co_3O_4-NWA, Co_3O_4-NTA and Co_3O_4-NTA at the current density of 2 mA/cm^2 (c); calculated area capacitance values from galvanostatic charge-discharge curves (d) and EIS plots (e) of Co_3O_4-NWA, Co_3O_4-CSNWA and Co_3O_4-NTA; the corresponding cycling stability of Co_3O_4-NWA, Co_3O_4-CSNWA and Co_3O_4-NTA at the current density of 20 mA/cm^2 after 5000 cycles (f)

The capacity values calculated from the galvanostatic charge-discharge curves are shown in Figure 4d. The area capacity (1.06 C/cm^2) of Co_3O_4-NTA at the current density of 40 mA/cm^2 still maintains up to 46.9% of that measured at 2 mA/cm^2 (2.26 C/cm^2). It was clear to observe the best rate capability of Co_3O_4-NTA especially from the converted massive specific capacity, Co_3O_4-NWA and Co_3O_4-CSNWA remained the initial capacitance of 11.2% and 20.4% with increasing the current density from 2 to 40 mA/cm^2, respectively. This was ascribed to the worse charge transport efficiency as confirmed by electrochemical impedance spectroscopy (EIS) test, the ohmic resistance of Co_3O_4-NTA (0.15 Ω) is much lower than 0.67 Ω of Co_3O_4-NWA and 0.39 Ω of Co_3O_4-CSNWA for (Figure 4e). Note that, Co_3O_4-NTA was comprised of the ultrathin Co_3O_4 nanoparticles in contrast to the bigger nanoparticles inside Co_3O_4-NWA and Co_3O_4-CSNWA; According with our previous observation, MnO_2 nanotube decorated with small Co_3O_4 nanoparticle layer demonstrated much better conductivity than the hybrid with big Co_3O_4 nanoparticles,[21] suggesting the very small nanoparticles to construct the architecture facilitated charge transfer of the materials. It was more preferable to choose building blocks with small particle size rather than those of big particles for the heterostructures of electrodes. Furthermore, Co_3O_4-NTA (580 C/g at 1.18 A/g, 298 C/g at 11.8 A/g) exhibited comparable or better specific capacity and rate capability in comparison with the reported Co_3O_4-based materials such as Co_3O_4 nanocube (297 C/g at 0.2 A/g, 136 C/g at 2 A/g),[53] Co_3O_4/graphene composite (384 C/g at 10 A/g, 273 C/g at 30 A/g),[54] Co_3O_4@MnO_2 core-shell nanowire array (384 C/g at 2.67 A/g, 213 C/g at 29.8 A/g),[41] Co_3O_4@PPy@MnO_2 core-shell-shell nanowire array (503 C/g at 0.33 A/g) [44] and Co_3O_4/PEDOT@MnO_2 core-shell nanowire array (391 C/g at 5 A/g), [55] indicating the excellent charge storage performance of our ZIF-67-derived Co_3O_4-NTA. The overall capacitance loss for Co_3O_4-NWA and Co_3O_4-CSNWA was respectively about 27.2% and 18.9% after 5000 cycles at a current density of 20 mA/cm^2 (Figure 4f), while Co_3O_4-NTA retained 96.9% of the initial capacity (1.46 C/cm^2). In addition, the resulting morphology of the electrodes shown in Figure S19 also confirmed the worst stability of Co_3O_4-NWA in which most of the Co_3O_4 nanowires were broken off and stacked into nanowire clusters. The above results demonstrated that Co_3O_4-NTA showed an outstanding cycling stability apart from the good specific capacity and rate capability. Furthermore, the use of Co_3O_4-NTA as the scaffold to build up other hybrid electrodes would further offer great enhancement in performance due to the specific structure and possible synergetic effect.[40]

Conclusions

In summary, water-insoluble inorganic crystalline Co-NWs have been successfully used as the precursor to synthesize ZIF-67 at room temperature in aqueous HMe-Im solution, resulting from the acid-base affinity between Co-NW and HMe-Im. The well-designed ZIF-67-based nanostructures with tunable morphologies have also been achieved by carefully controlling the conversion parameters. ZIF-67-derived architectures Co_3O_4-NTA and Co_3O_4-CSNWA shows much better electrochemical performances than the Co_3O_4 nanowire array directly converted from Co-NWs. This is due to the superiority of the specific structure, which affords high surface area, shortens ion diffusion path and facilitates the charge transfer. We believe the proposed strategy will open up a new avenue for the design and synthesis of MOF-based architectures, which broadens the extensive applications of MOFs; in addition, the as-obtained ZIF-67-based nanostructures will be excellent materials for other applications such as catalysts, sensors and energy conversion and storage devices.

Acknowledgements

This work was financially supported by the National Natural Science Foundation of China (Nos. 21490581) and National Basic Research Program of China (No. 2012CB932802).

Notes and references

†Electronic Supplementary Information (ESI) available: 1) Detailed experimental procedures and characterizations; 2) TEM images of cobalt carbonate hydroxide nanowires; 3) XRD patterns and Nitrogen adsorption–desorption isotherms of cobalt carbonate hydroxide nanowires and resulting materials after different reaction time; 4) Optical images of the conversion of cobalt carbonate hydroxide nanowire powder into ZIF-67 at room temperature and 75^{o}C by varying the reaction parameters; 5) SEM images of the precursor cobalt carbonate hydroxide nanowire arrays; 6) SEM images of resulting morphologies in different reaction condition; 7) XRD patterns of less-dense cobalt carbonate hydroxide nanowire nanowire array in present of 2-methylimidazole; 8) XRD patterns of ZIF-CSNWA, ZIF-NTA, Co_3O_4-CSNWA and Co_3O_4-NTA; TEM images of ZIF-CSNWA, Co_3O_4-CSNWA and ZIF-NTA; 9) Nitrogen adsorption–desorption isotherms of Co_3O_4-NWA, Co_3O_4-CSNWA and Co_3O_4-NTA; 10) Electrochemical properties of Co_3O_4-NWA, Co_3O_4-CSNWA and Co_3O_4-NTA. See DOI: 10.1039/x0xx00000x

1 H. Furukawa, K. E. Cordova, M. O'Keeffe and O. M. Yaghi, *Science*, 2013, **341**, 1230444.
2 H. Deng, C. J. Doonan, H. Furukawa, R. B. Ferreira, J. Towne, C. B. Knobler, B. Wang and O. M. Yaghi, *Science*, 2010, **327**, 846-850.
3 H.-C. J. Zhou and S. Kitagawa, *Chem. Soc. Rev.*, 2014, **43**, 5415-5418.
4 T. K. Kim, K. J. Lee, J. Y. Cheon, J. H. Lee, S. H. Joo and H. R. Moon, *J. Am. Chem. Soc.*, 2013, **135**, 8940-8946.
5 S. J. Yang, T. Kim, J. H. Im, Y. S. Kim, K. Lee, H. Jung and C. R. Park, *Chem. Mater.*, 2012, **24**, 464-470.
6 H. L. Jiang, B. Liu, Y. Q. Lan, K. Kuratani, T. Akita, H. Shioyama, F. Zong and Q. Xu, *J. Am. Chem. Soc.*, 2011, **133**, 11854-11857.
7 A. Aijaz, N. Fujiwara and Q. Xu, *J. Am. Chem. Soc.*, 2014, **136**, 6790-6793.
8 T. Rodenas, I. Luz, G. Prieto, B. Seoane, H. Miro, A. Corma, F. Kapteijn, F. X. L. i. Xamena and J. Gascon, *Nat. Mater.*, 2015, **14**, 48-55.
9 Z. Zhang, Y. Chen, S. He, J. Zhang, X. Xu, Y. Yang, F. Nosheen, F. Saleem, W. He and X. Wang, *Angew. Chem. Int. Ed.*, 2014, **53**, 12517-12521.
10 M. Zhao, K. Deng, L. He, Y. Liu, G. Li, H. Zhao and Z. Tang, *J. Am. Chem. Soc.*, 2014, **136**, 1738-1741.
11 P. Hu, J. V. Morabito and C.-K. Tsung, *ACS Catal.*, 2014, **4**, 4409-4419.
12 Y. Lu, W. Zhan, Y. He, Y. Wang, X. Kong, Q. Kuang, Z. Xie and L. Zheng, *ACS Appl. Mater. Interfaces*, 2014, **6**, 4186-4195.
13 J. M. Taylor, K. W. Dawson and G. K. Shimizu, *J. Am. Chem. Soc.*, 2013, **135**, 1193-1196.
14 J. Wang, H. X. Zhong, Y. L. Qin and X. B. Zhang, *Angew. Chem. Int. Ed.*, 2013, **52**, 5248-5253.
15 F. Zheng, Y. Yang and Q. Chen, *Nat. Commun.*, 2014, **5**, 5261.
16 X. Cao, B. Zheng, X. Rui, W. Shi, Q. Yan and H. Zhang, *Angew. Chem. Int. Ed.*, 2014, **53**, 1404-1409.
17 F. Zou, X. Hu, Z. Li, L. Qie, C. Hu, R. Zeng, Y. Jiang and Y. Huang, *Adv. Mater.*, 2014, **26**, 6622-6628.
18 P. Zhang, F. Sun, Z. Xiang, Z. Shen, J. Yun and D. Cao, *Energy Environ. Sci.*, 2014, **7**, 442-450.
19 Y. Hou, T. Huang, Z. Wen, S. Mao, S. Cui and J. Chen, *Adv. Energy Mater.*, 2014, **4**, 1400337.
20 J. Tang, R. R. Salunkhe, J. Liu, N. L. Torad, M. Imura, S. Furukawa and Y. Yamauchi, *J. Am. Chem. Soc.*, 2015, **137**, 1572-1580.
21 D. Yu, J. Yao, L. Qiu, Y. Wang, X. Zhang, Y. Feng and H. Wang, *J. Mater. Chem. A*, 2014, **2**, 8465-8471.
22 D. Yu, Y. Wang, L. Zhang, Z.-X. Low, X. Zhang, F. Chen, Y. Feng and H. Wang, *Nano Energy*, 2014, **10**, 153-162.
23 C. Li, T. Sato and Y. Yamauchi, *Angew. Chem. Int. Ed.*, 2013, **52**, 8050-8053.
24 C. Guan, J. Liu, C. Cheng, H. Li, X. Li, W. Zhou, H. Zhang and H. J. Fan, *Energy Environ. Sci.*, 2011, **4**, 4496-4499.
25 H. Hu, L. Yu, X. Gao, Z. Lin and X. W. D. Lou, *Energy Environ. Sci.*, 2015, **8**, 1480-1483.
26 N. Yanai and S. Granick, *Angew. Chem. Int. Ed.*, 2012, **51**, 5638-5641.
27 N. Yanai, M. Sindoro, J. Yan and S. Granick, *J. Am. Chem. Soc.*, 2013, **135**, 34-37.
28 S. Tanaka, K. Kida, T. Nagaoka, T. Ota and Y. Miyake, *Chem. Commun.*, 2013, **49**, 7884-7886.
29 G. Majano and J. Perez-Ramirez, *Adv. Mater.*, 2013, **25**, 1052-1057.
30 L. X. Ding, A. L. Wang, G. R. Li, Z. Q. Liu, W. X. Zhao, C. Y. Su and Y. X. Tong, *J. Am. Chem. Soc.*, 2012, **134**, 5730-5733.
31 Z. Chen, M. Waje, W. Li and Y. Yan, *Angew. Chem. Int. Ed.*, 2007, **119**, 4138-4141.
32 B.-S. Choi, Y. W. Lee, S. W. Kang, J. W. Hong, J. Kim, I. Park and S. W. Han, *ACS Nano*, 2012, **6**, 5659-5667.
33 H. Zhang, M. Jin, J. Wang, W. Li, P. H. Camargo, M. J. Kim, D. Yang, Z. Xie and Y. Xia, *J. Am. Chem. Soc.*, 2011, **133**, 6078-6089.
34 A. F. Gross, E. Sherman and J. J. Vajo, *Dalton Trans.*, 2012, **41**, 5458-5460.
35 J. Yao, M. He, K. Wang, R. Chen, Z. Zhong and H. Wang, *CrystEngComm*, 2013, **15**, 3601-3606.
36 G. Saracco, S. Vankova, C. Pagliano, B. Bonelli and E. Garrone, *Phys.Chem.Chem.Phys.*, 2014, **16**, 6139-6145.
37 M. C. McCarthy, V. Varela-Guerrero, G. V. Barnett and H.-K. Jeong, *Langmuir*, 2010, **26**, 14636-14641.
38 J. Cravillon, S. Mu¨nzer, S.-J. Lohmeier, A. Feldhoff, K. Huber and M. Wiebcke, *Chem. Mater.*, 2009, **21**, 1410-1412.
39 W. Zhou, X. Cao, Z. Zeng, W. Shi, Y. Zhu, Q. Yan, H. Liu, J. Wang and H. Zhang, *Energy Environ. Sci.*, 2013, **6**, 2216–2221.
40 X. Gu, L. Chen, Z. Ju, H. Xu, J. Yang and Y. Qian, *Adv. Funct. Mater.*, 2013, **23**, 4049–4056.
41 J. Liu, J. Jiang, C. Cheng, H. Li, J. Zhang, H. Gong and H. J. Fan, *Adv. Mater.*, 2011, **23**, 2076-2081.
42 S. H. Ko, D. Lee, H. W. Kang, K. H. Nam, J. Y. Yeo, S. J. Hong, C. P. Grigoropoulos and H. J. Sung, *Nano Lett.*, 2011, **11**, 666-671.
43 B. U. Ye, B. J. Kim, J. Park, H. Y. Jeong, J. Y. Park, J. K. Kim, J.-H. Hur, M. H. Kim, J.-L. Lee and J. M. Baik, *Adv. Funct. Mater.*, 2014, **24**, 3384-3391.
44 L. Han, P. Tang and L. Zhang, *Nano Energy*, 2014, **7**, 42-51.
45 E. Gonzalez, J. Arbiol and V. F. Puntes, *Science*, 2011, **334**, 1377-1380.
46 S. R. Venna, J. B. Jasinski and M. A. Carreon, *J. Am. Chem. Soc.*, 2010, **132**, 18030–18033.
47 J.-H. Zhong, A.-L. Wang, G.-R. Li, J.-W. Wang, Y.-N. Ou and Y.-X. Tong, *J. Mater. Chem.*, 2012, **22**, 5656-5665.
48 X.-h. Xia, J.-p. Tu, Y.-q. Zhang, Y.-j. Mai, X.-l. Wang, C.-d. Gu and X.-b. Zhao, *RSC Adv.*, 2012, **2**, 1835-1841.
49 B. Wang, T. Zhu, H. B. Wu, R. Xu, J. S. Chen and X. W. Lou, *Nanoscale*, 2012, **4**, 2145-2149.
50 Z. Jiang, Z. Li, Z. Qin, H. Sun, X. Jiao and D. Chen, *Nanoscale*, 2013, **5**, 11770-11775.
51 X. Xu, R. Cao, S. Jeong and J. Cho, *Nano Lett.*, 2012, **12**, 4988-4991.
52 A. Banerjee, U. Singh, V. Aravindan, M. Srinivasan and S. Ogale, *Nano Energy*, 2013, **2**, 1158-1163.
53 X. Liu, Q. Long, C. Jiang, B. Zhan, C. Li, S. Liu, Q. Zhao, W. Huang and X. Dong, *Nanoscale*, 2013, **5**, 6525–6529.

54 X.-C. Dong, H. Xu, X.-W. Wang, Y.-X. Huang, M. B. Chan-Park, H. Zhang, L.-H. Wang, W. Huang and P. Chen, *ACS Nano*, 2012, **6**, 3206–3213.
55 X. Xia, D. Chao, Z. Fan, C. Guan, X. Cao, H. Zhang and H. J. Fan, *Nano Lett.*, 2014, **14**, 1651-1658.

TOC image

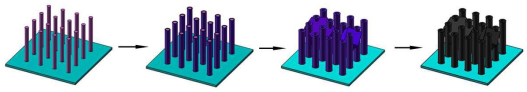

A facile transformation to ZIF-67-based nanotube array supported on Ni foam was achieved by simply immersing cobalt carbonate hydroxide nanowire array into 2-methylimidazole and triethylamine aqueous solution. After annealing treatment, the ZIF-67-derived mesoporous Co_3O_4 nanotube array was further prepared, which composed of all the ultrathin Co_3O_4 nanoparticles and thus exhibited remarkable electrochemical performances as battery-type electrode due to the unique structure.